Quasi-flat high-index acoustic lens for 3D underwater ultrasound focusing

Olivier Lombard, Raj Kumar, Olivier Mondain-Monval, Thomas Brunet, Olivier Poncelet

Applied Physics Letters

Quasi-flat high-index acoustic lens for 3D underwater ultrasound focusing

Cite as: Appl. Phys. Lett. **120**, 221701 (2022); https://doi.org/10.1063/5.0088503
Submitted: 17 February 2022 • Accepted: 12 May 2022 • Published Online: 31 May 2022

Olivier Lombard, Raj Kumar, Olivier Mondain-Monval, et al.

AIP Publishing

Applied Physics Letters ARTICLE scitation.org/journal/apl

Quasi-flat high-index acoustic lens for 3D underwater ultrasound focusing

Cite as: Appl. Phys. Lett. **120**, 221701 (2022); doi: 10.1063/5.0088503
Submitted: 17 February 2022 · Accepted: 12 May 2022 ·
Published Online: 31 May 2022

Olivier Lombard,[1,a)] Raj Kumar,[2] Olivier Mondain-Monval,[2,b)] Thomas Brunet,[1,b)] and Olivier Poncelet[1]

AFFILIATIONS

[1]University Bordeaux, CNRS, Bordeaux INP, ENSAM, UMR 5295 I2M, F-33405 Talence, France
[2]University Bordeaux, CNRS, UMR 5031 CRPP, F-33600 Pessac, France

Note: This paper is part of the APL Special Collection on Acoustic and Elastic Metamaterials and Metasurfaces.
[a)]**Present address:** University Avignon, UMR 1114 EMMAH, Avignon, France.
[b)]**Authors to whom correspondence should be addressed:** olivier.mondain@crpp.cnrs.fr and thomas.brunet@u-bordeaux.fr

ABSTRACT

We report a quasi-flat and sub-wavelength acoustic lens built using a soft matter process for broadband ultrasonic 3D focusing in water. By using a simple emulsion templating method, a soft porous material with a high acoustic index relative to water (∼5) has been molded and shaped into a convergent lens with a very low curvature and a thickness smaller than the working wavelength in water. This kind of acoustic metasurface generates a narrow focused beam, and its focal length can be adjusted. These acoustic lenses may be of great interest for underwater applications, where acoustic focusing and imaging are highly demanded.

Acoustic focusing is a major issue in many applications such as medical diagnosis, underwater acoustics, nondestructive testing, and many other fields.[1] As recently reviewed by Ma *et al.*,[2] the focusing of acoustic waves can be achieved thanks to traditional methods using acoustic lenses or using speaker/transducer arrays and time-reversal mirrors. The first lens-based focusing approach might be interesting for some applications since it does not require any sophisticated and costly electronic devices. Moreover, new artificial structures such as phononic crystals,[3] acoustic metamaterials,[4,5] or acoustic metasurfaces[6] have been recently proposed to fabricate various new-concept focusing lenses, including anisotropic density-near-zero hyperlens,[7] negative-index superlens,[8] and sub-wavelength lenses with phase gradients.[9] However, the acoustic lenses most commonly used in the industry remain to this day very simple devices such as gradient cross-sectional acoustic lenses that are similar to convex and concave optical lenses.[2] According to Snell's laws, sound waves are refracted when passing through the curved acoustic lens because of the sound speed (or acoustic index) contrast with the surrounding medium. Thus, the device is changing the propagation direction of the incident waves, and this direction depends on the curvature and the acoustic index of the lens. For 3D sound focusing in free space, these acoustic lenses are usually spherical structures and have been studied in detail for a long time.[10] In underwater acoustics, these acoustic devices are usually made of stiff materials such as rigid polymers, or even glass, having an acoustic index close to that of water. Such a low acoustic index contrast between the acoustic lens and the surrounding medium, thus, leads to thick and highly curved lenses, which can be a problem in many applications.[11] In this paper, we, thus, re-examine the concept of a classical curved lens having a high acoustic index, so as to get the thinnest and flattest possible device in the spirit of the recent concept of acoustic metasurfaces whose thicknesses have to be lower than the incident acoustic wavelength.[12]

Our technique involves the use of a macro-porous soft polymer to build up the metasurface. As has been well established, the longitudinal sound speed inside a porous material depends on its porosity.[13] In soft rubber, i.e., a polymer material exhibiting a glass transition temperature T_G much lower than room temperature, the sound velocity decreases dramatically, falling down from ∼1000 to 100 m/s as the porosity only slightly increases from 0 to a few percent.[14] Such low velocities are the consequence of the high values of the ratio K/G (where K and G are, respectively, the polymer bulk elastic and shear storage moduli), which is the main key parameter in this issue as well described by a quasi-static model.[15] In a recent study,[16] we used this dependence to build up a gradient index flat acoustic lens by introducing a gradient of porosity in the material. In this paper, we build a lens that exhibits a non-zero curvature and a uniform value of the acoustic index $n = c_W/c$ (with c_W and c, respectively, the sound speeds in water, 1482 m/s, and inside the lens). The geometry of the axisymmetric lens

is shown in Fig. 1. One face is planar with a circular section of radius a while the other one exhibits a curvature defined by the function $r(\theta) = \|\vec{r}\|$ ($\vec{r}$ and θ being defined in Fig. 1). First, using well established equations for the propagation and the refraction of waves,[17] we will establish its expression as a function of the targeted focal length F and acoustic index n and then we will choose the experimental parameters so as to obtain the targeted properties.

The problem is described in Fig. 1. The planar wave emitted by the flat ultrasonic (US) transducer travels through the lens and is focused in water toward the point P at a distance F from the center O of the lens (i.e., OP = F). We first use a classical approach to describe the path followed by the acoustic beam. With the aim of finding the lens geometry producing a geometrical focusing at the point P, let us consider an acoustic ray that propagates within the lens along the z-axis from point H (on the flat face) to point M (on the curved face) located at the interface with the surrounding fluid and that is refracted toward point P. In this approach, we neglect the multiple reflections that occur in the porous lens because of its absorption.[15] The following development is based on the classical approach of wave propagation.[17] The time of flight $\tau(HP)$ corresponding to the acoustic path from H to P via point M reads

$$\tau(HP) = \tau(HM) + \tau(MP) = \frac{F - r\cos\theta}{c} + \frac{r}{c_W}, \tag{1}$$

where $r = |\mathrm{PM}|$ and θ is the angle between PO and PM. Within the scope of the Fermat principle, geometrical focusing at P is obtained for a stationary time of flight $\tau(HP)$ with respect to all positions of points H and M, that is, for $d\tau(HP) = 0$. The latter condition defines the geometry $r(\theta)$ of the focusing lens hence having a radially dependent thickness. Additionally, we aim at making a lens with a near-zero thickness at the edge (points M and H merging when $OH = a$) that provides a constraint on the lens geometry function $r(\theta)$

$$r(\theta_{max}) = \sqrt{a^2 + F^2}, \tag{2}$$

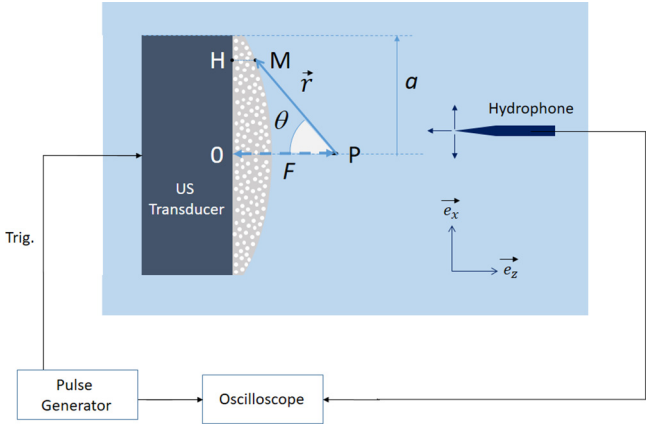

FIG. 1. Schematic presentation of the z-axisymmetric lens on its transducer: definition of the different variables and points used in the text; the incident plane wave is emitted by an ultrasonic transducer and goes through the lens along the z direction. Three different transducers, of sizes 1 in. in diameter, are used with central frequencies centered at 200, 500, and 1000 kHz. The whole system is immersed in water. A hydrophone scans the pressure field in the (x, z) plane, and the signal is recorded by the oscilloscope.

where $\theta_{max} = \mathrm{atan}(a/F)$ is the maximal achievable value of θ. A stationary time of flight coupled with this constraint leads to the following expression of $r(\theta)$, which describes the curved surface of the lens:

$$r(\theta) = \frac{nF - \sqrt{a^2 + F^2}}{n\cos(\theta) - 1}. \tag{3}$$

The curved surface of the lens, of the symmetry axis OP, is a hyperboloid. The eccentricity of the hyperboloid is equal to the acoustic index n of the quasi-flat lens.

Here, the radius a of the lens is set to 12.7 mm as a geometrical constraint in order to fit the acoustic transducer (1 inch-diameter), and we target a focal distance F of 15 mm. With an acoustic index $n = 5$, it implies a maximal thickness of 1.1 mm at the center of the lens.

The lens was obtained by first fabricating a mold having the geometrical form of a hyperboloid following Eq. (3). Because of the brittleness of the used soft porous polymer materials, an extra layer of 200 μm was added onto the flat interface for avoiding breaking or failures on the edges. However, it is worth noting that despite this excess thickness of the lens, its maximal total thickness (here 1.3 mm) is still smaller than the smallest incident acoustic wavelength in the surrounding medium, which is water in our experiments (thus $f < 1$ MHz means that $\lambda_w > 1.5$ mm), which justifies its classification as a metasurface.[6] The used procedure to build the lens is shown in Fig. 2. As compared to our previous work on the GRIN lens,[16] the building procedure only involves one homogeneous medium with a given porosity value.

The mold is built using a 3D printing method and is made of polylactic acid (PLA). We then used soft porous polydimethylsiloxane (PDMS) to build up the body of the lens. This material is obtained by using the emulsion templating recipes described in our earlier publications.[14–16,18] Shortly, a controlled amount of water is emulsified into an initial liquid mixture composed of PDMS and a surfactant. The emulsion volume fraction ϕ_{emulsion} is the ratio of the introduced volume of water and the total volume. The obtained water droplets exhibit a Gaussian size distribution of diameters comprised typically between 1 and 10 μm (much smaller than the ultrasonic acoustic wavelength in the final porous material). The obtained water-in-PDMS emulsion is then poured into the PLA mold and is further exposed to UV during typically 10 min, which triggers the cross-linking of the PDMS phase [Fig. 2(a)]. The obtained water-in-rubber system is then subjected to a drying process using supercritical CO_2 (fully detailed in Ref. 18). Thus, water is driven out of the pores and replaced by air, and one obtains a lens [Fig. 2(b)] made with rubber exhibiting a porosity $\phi = \phi_{\mathrm{emulsion}}$. We targeted a porosity value $\phi = 5 \pm 1\%$ to reach the targeted value of the acoustic index ($n \approx 5$). However, the porous material being slightly dispersive, we first measured precisely its sound speed as a function of frequency f between 100 and 400 kHz using a procedure fully described earlier[19] and then extrapolated the relation between phase velocity and frequency. Doing so, we measured a sound speed c (m/s) = 0.2325 f (kHz) + 216.4, which corresponds to $n = 5.2$ at 300 kHz and 3.7 at 800 kHz. We also measured its attenuation coefficient α as a function of frequency f providing $\alpha\,(\mathrm{mm}^{-1}) = 5.4 \times 10^{-3} f\,(\mathrm{kHz})$.

We now describe the experimental setup (Fig. 1) that was used to evidence the focusing ability of the quasi-flat lens. The active surface of

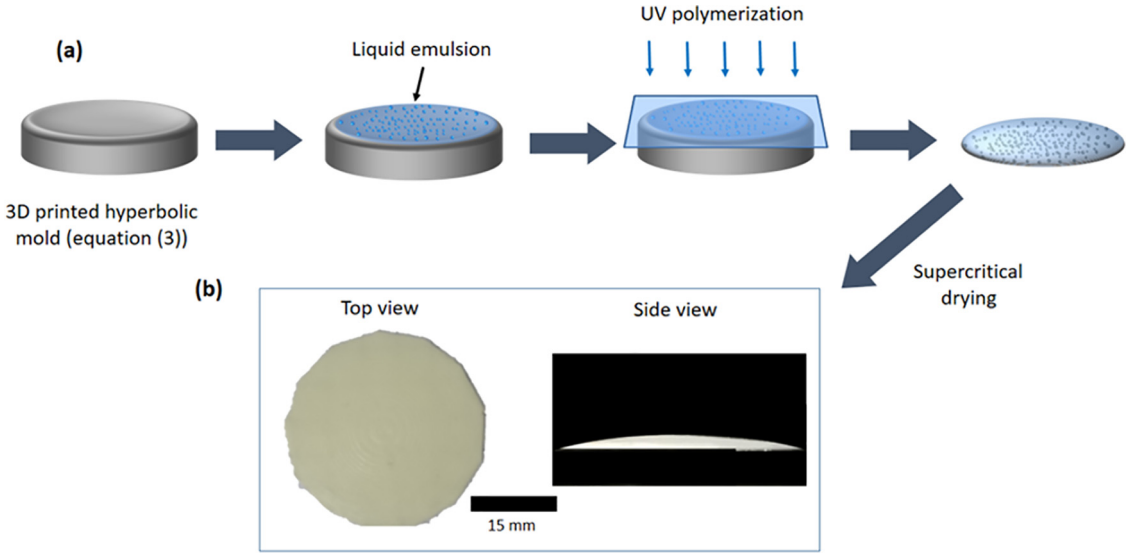

FIG. 2. (a) Procedure of the lens synthesis: the liquid emulsion is poured into the PLA mold having the shape of a hyperboloid surface of Eq. (3). The emulsion is then cross-linked using UV, and the solid lens is then unmolded and subjected to supercritical drying. (b) Top (left) and side (right) views of the lens with one hyperbolic surface (up) and one flat interface (bottom interface).

the US transducer is in contact with the flat side of the lens while the hyperbolic side is in contact with the water. The US transducer is excited with a short broadband electrical pulse and emits an acoustic wavepacket that first propagates inside the lens before being radiated in water. A hydrophone, driven by a controller, records the transmitted signal at different positions in the $(x–z)$ plane. The origin point ($x = 0$ and $z = 0$) of this coordinate system is in point O. We then obtain a map of the pressure field radiated from the lens. The cartography is made from $x = -17$ to $x = 17$ mm in the x-direction (perpendicular to the lens symmetry axis) and to $z = 80$ mm in the z direction (symmetry axis). The recorded points are separated from each other by a sub-wavelength step distance of 0.25 mm. The scans were performed without and with the porous lens. Measurements used three transducers with central frequencies of 200, 500 kHz, and 1 MHz, to access a broad range of frequencies lying between 250 kHz and 800 MHz. The measured data could not be obtained at f larger than 800 kHz due to the large attenuation of the material at high frequency. At each (x, z)-position, the signals are Fourier transformed, and the cartography of the pressure field can be plotted in both cases (without and with the porous lens). As an example, Figs. 3(a) and 3(b) show the pressure field maps for a central frequency of 800 kHz. Without the lens, we observe a wide spot spreading around $z = 80$ mm that is due do the transducer finite size diffraction effect. A complex near field pattern with several regions of intensities comparable to the one of the wider spot is also observed at shorter distance.

With the lens, one observes only one focal point located at $z = 25$ mm, and the complex near field pattern is no longer observed at distances shorter than 25 mm. This mismatch between the measured focal length (25 mm) and the targeted one (15 mm) is due to the dependence of the acoustic index on the frequency and to a focal shift effect.[20] The z and x profiles passing through this focal point are plotted in Figs. 3(c) and 3(d).

To get the solid lines of Figs. 3(c) and 3(d), we used the following theoretical approach. First, we can write the following Rayleigh integral:

$$P(\vec{r}_0) = j\rho 2\pi f \iint_S v_n(\vec{r}) \frac{e^{jk_0|\vec{r}_0 - \vec{r}|}}{2\pi|\vec{r}_0 - \vec{r}|} d^2S, \tag{4}$$

which evaluates the pressure field $P(\vec{r}_0)$ at a point $\vec{r}_0$ radiated in the surrounding medium by the entire lens-surface S locating all the points $\vec{r}$ of emission on the hyperboloid surface. ρ and k_0 are, respectively, the material mass density and the wavenumber in the surrounding medium (water in this case) and $v_n(\vec{r})$ is the acoustic velocity field normal to the surface S, which reads

$$v_n(\vec{r}) = v_0 \frac{e^{jnk_0 z(r)}}{\sqrt{1 + (dz/dr)^2}}, \tag{5}$$

where v_0 is the uniform value of the forced normal velocity at the ultrasonic transducer surface in contact with the flat side of the lens and $z(r)$ is the thickness of the lens at the position $\vec{r} = r\vec{PM}/|\vec{PM}|$ on the surface. The exponential argument $jnk_0z(r)$ in (5) describes the phase of the traveling wavefront within the lens, and the denominator comes from the angle between the normal vector and the z-axis at position $\vec{r}$ on the surface. Using these two equations, one can compute the pressure field at each point of the (x, z) plane for each frequency. The experimental and calculated values of the maximum of the z profile, which is the focal length F of the lens, and the full width at half maximum (FWHM) of the x profiles (around the focal point) are plotted as a function of frequency in Figs. 4(a) and 4(b). The confidence bars on the position of the focal point and on the FWHM values come from the uncertainty that we estimate to be at 5%, on the maximum intensity measurements in Figs. 3(c) and 3(d). From Figs. 4(a) and 4(b), it appears that the used model is in very good agreement with the

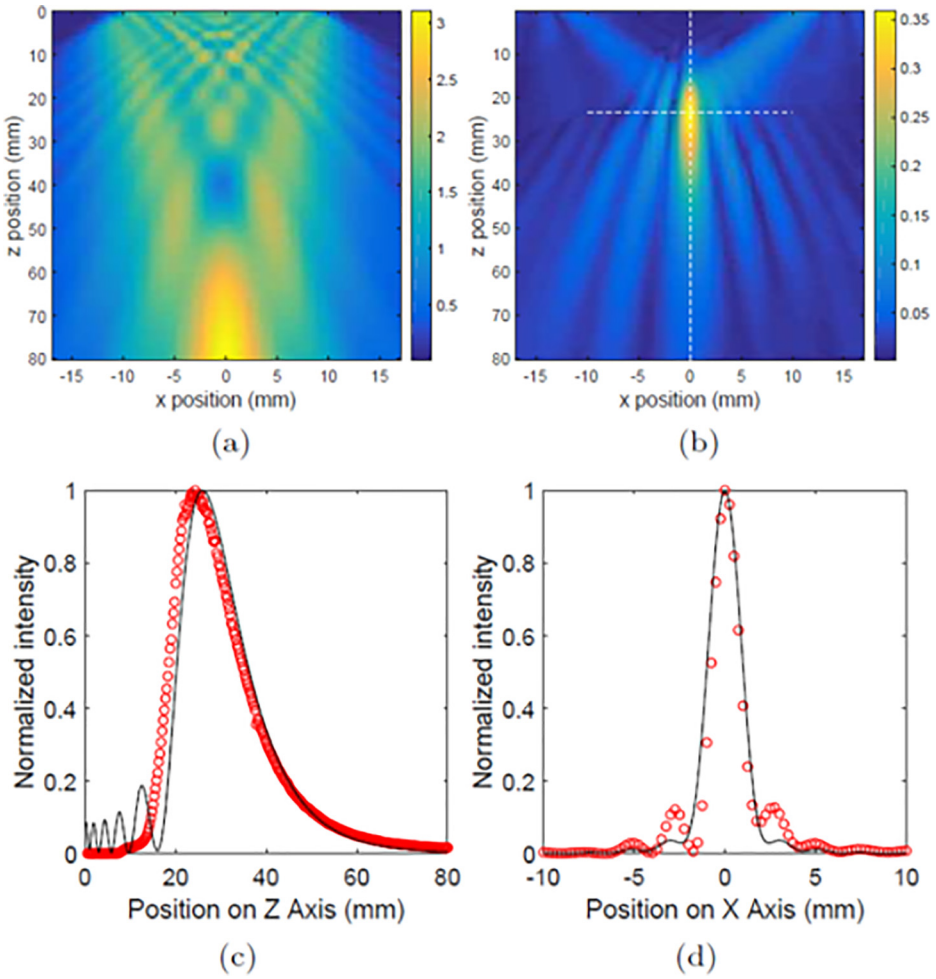

FIG. 3. (a) and (b) Acoustic field patterns extracted from fast Fourier transforms performed at 800 kHz in the (x, z) plane recorded without the lens (a) and with the lens (b). The dotted white lines are the z and x profiles along which the intensity of the pressure field is recorded and plotted in (c) and (d), respectively. (c) and (d) Normalized intensity of the pressure field at 800 kHz along the z (c, at $x = 0$) and x (d, at $z = 25$ mm) profiles. The experimental points are the empty red circles, and the solid lines are the calculated value obtained using Eqs. (3) and (4) in the text.

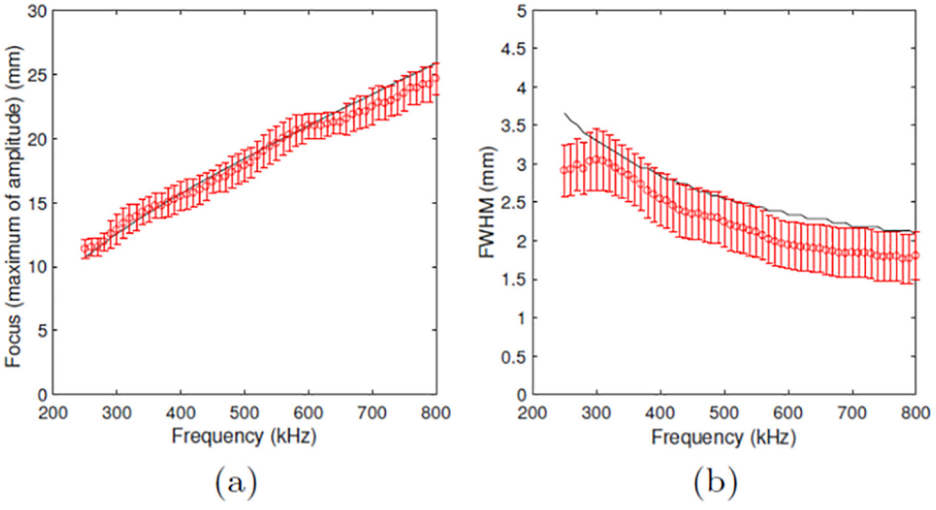

FIG. 4. Evolution of the focal length F at $x = 0$ (a) and of the FWHM values of the x profiles (b) as a function of frequency. The red empty circles are the experimental points, and the solid lines are obtained using the model described in the text.

experimental data and exhibits the correct trends within experimental uncertainty. The experimental FWHM values of the spot vary from 0.6λ at 300 kHz (3 mm) to 0.9λ at 800 kHz (1.7 mm). These values are very similar to the ones obtained with a gradient index lens made with the same type of material (one found 0.8λ at 200 kHz in Ref. 16). Such values of the FWHM is around the diffraction limit. The focus distance of the spot is around 2λ at 300 kHz, but it increases with frequency to the value 10λ at 800 kHz. Also, the focal length of the lens can be adjusted by simply playing with the porosity value of the medium, which can be targeted to reach higher index values (up to ~ 40[15]), thus lower focal lengths, or equivalently, flatter devices. This device is cheap, very simple to fabricate, highly versatile, and is an alternative to the soft gradient index metasurfaces.[16] Its characteristics can be adjusted to various types of transducers and values of focal distance over a broad range of frequencies in the ultrasonic underwater domain.

We thank Frédéric Marchal and Tania Ireland from Elkem Company for fruitful discussions and for providing us with silicone rubber. This study received financial support from the French government in the framework of the University of Bordeaux's IdEx "Investments for the Future" program/GPR PPM and project BRENNUS ANR-15-CE08-0024.

AUTHOR DECLARATIONS

Conflict of Interest

The authors have no conflicts to disclose.

DATA AVAILABILITY

The data that support the findings of this study are available from the corresponding authors upon reasonable request.

REFERENCES

[1]D. R. Raichel, *The Science and Applications of Acoustics* (Springer Science & Business Media, 2006).
[2]F. Ma, Z. Huang, C. Liu, and J. H. Wu, "Acoustic focusing and imaging via phononic crystal and acoustic metamaterials," J. Appl. Phys. **131**(1), 011103 (2022).
[3]A. Khelif and A. Adibi, *Phononic Crystals* (Springer, Berlin, 2015).
[4]S. A. Cummer, J. Christensen, and A. Alù, "Controlling sound with acoustic metamaterials," Nat. Rev. Mater. **1**(3), 16001 (2016).
[5]G. Ma and P. Sheng, "Acoustic metamaterials: From local resonances to broad horizons," Sci. Adv. **2**(2), e1501595 (2016).
[6]B. Assouar, B. Liang, Y. Wu, Y. Li, J. C. Cheng, and Y. Jing, "Acoustic metasurfaces," Nat. Rev. Mater. **3**(12), 460–472 (2018).
[7]Y. Gu, Y. Cheng, and X. Liu, "Acoustic planar hyperlens based on anisotropic density-near-zero metamaterials," Appl. Phys. Lett. **107**(13), 133503 (2015).
[8]N. Kaina, F. Lemoult, M. Fink, and G. Lerosey, "Negative refractive index and acoustic superlens from multiple scattering in single negative metamaterials," Nature **525**(7567), 77–81 (2015).
[9]Y. Xie, W. Wang, H. Chen, A. Konneker, B. I. Popa, and S. A. Cummer, "Wavefront modulation and subwavelength diffractive acoustics with an acoustic metasurface," Nat. Commun. **5**(1), 5553 (2014).
[10]W. J. Toulis, "Acoustic focusing with spherical structures," J. Acoust. Soc. Am. **35**(3), 286–292 (1963).
[11]A. Briggs, "Acoustic microscopy-a summary," Rep. Prog. Phys. **55**(7), 851 (1992).
[12]J. Chen, J. Rao, D. Lisevych, and Z. Fan, "Broadband ultrasonic focusing in water with an ultra-compact metasurface lens," Appl. Phys. Lett. **114**(10), 104101 (2019).
[13]J.-F. Allard, *Propagation of Sound in Porous Media* (Springer, The Netherlands, 1993); L. W. Hrubesh, "Aerogel applications," J. Non-Cryst. Solids **225**, 335–342 (1998).
[14]A. Kovalenko, M. Fauquignon, T. Brunet, and O. Mondain-Monval, "Tuning the sound speed in macroporous polymers with a hard or soft matrix," Soft Matter **13**(25), 4526–4532 (2017).
[15]A. Ba, A. Kovalenko, C. Aristégui, O. Mondain-Monval, and T. Brunet, "Soft porous silicone rubbers with ultra-low sound speeds in acoustic metamaterials," Sci. Rep. **7**(1), 40106 (2017).
[16]Y. Jin, R. Kumar, O. Poncelet, O. Mondain-Monval, and T. Brunet, "Flat acoustics with soft gradient-index metasurfaces," Nat. Commun. **10**(1), 143 (2019).
[17]M. Born and E. Wolf, *Principles of Optics: 7th Anniversary Edition* (Cambridge University Press, 2019).
[18]R. Kumar, Y. Jin, S. Marre, O. Poncelet, T. Brunet, J. Leng, and O. Mondain-Monval, "Drying kinetics and acoustic properties of soft porous polymer materials," J. Porous Mater. **28**(1), 249–259 (2021).
[19]K. Zimny, A. Merlin, A. Ba, C. Aristégui, T. Brunet, and O. Mondain-Monval, "Soft porous silicone rubbers as key elements for the realization of acoustic metamaterials," Langmuir **31**(10), 3215–3221 (2015).
[20]Y. Gao, J. Liu, X. Zhang, Y. Wang, Y. Song, S. Liu, and Y. Zhang, "Analysis of focal-shift effect in planar metallic nanoslit lenses," Opt. Express **20**(2), 1320–1329 (2012).